DYNAMICS OF THE WEDDELL SEA ANOMALY AND THE MAIN IONOSPHERIC DIP IN THE SOUTHERN SUMMER HEMISPHERE

© 2025 A. T. Karpachev

Institute of Terrestrial Magnetism, Ionosphere and Radio Wave Propagation

Pushkov Institute of the Russian Academy of Sciences (IZMIRAN), Moscow, Troitsk, Russia

e-mail: karp@izmiran.ru

Received May 31, 2024

Revised July 16, 2024

Accepted July 25, 2024

The effect of the Weddell Sea anomaly on the structure of the nighttime ionosphere in the Southern summer hemisphere is studied. For this purpose, we used data from the CHAMP satellite for Januaryь 2003 with high solar activity and for January 2008 with low solar activity. The data relate to the local time interval 02–04 LT, when the strongest increase in the electron concentration occurs due to the formation of an anomaly. At longitudes 60–180180 180° E with high solar activity and 0–225° E with low solar activity, where the anomaly is absent, the main ionospheric dip is observed. The plasma peak in the nighttime ionosphere associated with the formation of the Weddell Sea anomaly reaches 6 MHz at low and 10 MHz at high solar activity. The strongly developed plasma peak at high solar activity decreases sharply to high latitudes at the equatorial boundary of auroral diffuse eruptions, which corresponds to the plasmopause. With a poorly developed anomaly, the contribution of diffuse eruptions becomes noticeable, so the plasma peak expands to the pole due to these eruptions. More polar than the anomaly, a high-latitude dip is usually observed at the latitudes of the auroral oval. Equatorial to the anomaly, a well-defined minimum of electron concentration is often formed, which can be defined as a subplot. It is shown that in some cases the subplot is associated with the removal of ionospheric plasma from the summer hemisphere to the winter one. Then, in the winter hemisphere, a maximum concentration is formed at conjugate latitudes. Subpopulation is much more often observed at low solar activity than at high solar activity.

DOI: 10.31857/S00167940250108e4

1. INTRODUCTION

At ionospheric stations Halley Bay (75.6° S, 333.4° E, 65.8° GMLat) and Argentine Island (65.3° S, 295.7°E, 53.8° GMLat) was first detected anomalous behavior of *foF*2: during the December solstice night values greatly exceed the daytime [Bellchambers and Piggott, 1958; Penndorf, 1965; Dudeney and Piggot, 1978]. Based on the name of the nearest sea, this effect was called the Weddell Sea Anomaly (Weddell Sea Anomaly, WSA). Studies of WSA characteristics were later continued using the TOPEX/Poseidon experiment for all levels of solar activity and all seasons [Horvath and Essex, 2003; Horvath, 2006; Jee et al., 2009], direct measurements *of the Ni ion concentration* at DMSP satellite altitude of 850 km [Horvath and Lovell, 2009], and *Ne electron concentrations* at the CHAMP satellite altitude of 400 km [Liu et al., 2010], as well as according to radio-eclipse measurements in the COSMIC/Formosat experiment [Burns et al., 2008; He et al., 2009; Lin et al., 2009]. The anomaly region was clearly delineated by data from the Intercosmos-19 and CHAMP satellites in [Karpachev et al., 2011 and Klimenko et al., 2015]. In all the cited works, the causes of the formation of anomalies were also discussed. A detailed study of the anomaly formation mechanism based on data from ground stations and the FLIP model was conducted in a recent study [Richards et al., 2018]. The main reason for a strong increase in the electron concentration at night at the latitudes of the anomaly is the effect of a neutral wind in the presence of high residual ionization after the" shutdown " of solar radiation.

The main ionospheric sinkhole (GIP) was discovered and described in the pioneering work of Muldrew [1965]. In addition to the GIP, Muldrew observed another dip at higher latitudes, which he identified as a high-latitude ionospheric dip. Both failures have been repeatedly investigated, and the results are presented in reviews [Ahmed et al., 1979; Moffett and Quegan, 1983; Grebowsky et al., 1983; Williams and Jain, 1986; Rodger et al., 1992; Nilsson et al., 2005]. As the study of both dips progressed, it was found that the VIP is located within the auroral oval of the eruptions [Grebowsky et al., 1983], and the IP is mainly located equatorial to the oval [Ahmed et al., 1979]. However, a VIP located at the lowest possible latitude can be confused with a VIP located at the highest possible latitude. Therefore, a special method using the auroral oval model was proposed to separate VIP and GIP [Vorobjev et al., 2013]. This model was developed using data from DMSP satellites at the Polar Geophysical Institute in Murmansk and is available on the website http://apm.pgia.ru. The model describes zone I of auroral diffuse eruptions on the equatorial edge of the auroral oval and zone II of diffuse eruptions on its polar edge. It has been shown that zone I usually forms the polar wall of the IPU, while zone II forms the polar wall of the IPU. This is a key factor in distinguishing GIP from VIP. The analysis is most effective within the framework of the longitude effect, since the position of all ionospheric structures depends on longitude. The position of the auroral oval also depends on longitude and is determined by the angle of inclination of the

Earth's dipole [Karpachev, 2023]. The amplitude of longitudinal variations in the auroral oval of eruptions is ~2.5°.

GIP is most pronounced in winter night conditions. However, at night it is quite well manifested in the summer. In the Southern summer hemisphere, the dynamics of the sinkhole should be strongly affected by the Weddell Sea anomaly. The purpose of this study is to test this assumption.

2. DATA

We used data from direct measurements of the *Ne* electron concentration on the CHAMP satellite [Rother and Michaelis, 2019]. Data were collected for–January 5-11, 2003 at high solar activity ($F10.7$ ~ 160 sfu) and for–January 3-13, 2008 at low solar activity ($F10.7$~80 sfu). The data relate to relatively quiet periods of time with $Kp < 4$. The satellite was orbiting in an almost polar orbit with an inclination of 87°, and the orbit height was ~520 km in January 2003 and ~360 km in January 2008. The *Ne* variations are presented below in terms of the plasma frequency *fp.* The measurements were carried out at ~1° latitude intervals, which makes it possible to determine the positions of all ionospheric structures fairly accurately. Data from the CHAMP satellite is freely available on the website (https://isdc.gfz-potsdam.de/champ-isdc://isdc.gfz-potsdam.de/champ-isdc/).

3. DISTRIBUTION OF ELECTRON CONCENTRATION IN THE SOUTHERN HEMISPHERE

Figure 1 shows the distribution *of fp* in the Southern Hemisphere for 02–04 LT obtained from CHAMP data for high solar activity (HSA) and low solar activity (LSA). The maps are based on data for several quiet days in January 2003 and January 2008, respectively. The *fp* values are much higher at ICA than at NSA, although at low activity the satellite was closer to the maximum *F* of the F2 layer. However, both distributions are similar in structure. In both cases, there is a strong increase in the electron concentration associated with the formation of WSA: at longitudes from 180° W до 70°W W to 70 E E at ICA, and from 150° W to 70° E at HSA. The anomaly is much more developed in ICA. The dashed curve shows the position of the GIP defined for 04 LT, but in winter conditions. As a result of data averaging, the summer GIP is clearly shown on maps only at longitudes 90-150 ° E–150° for ICA and at longitudes 60-210□ E for–210° NSA. VIP clearly manifested itself only at ICA at longitudesoϕ 120180° 180 E. E. Thus, a comparison of the electron concentration distributions for high and low solar activity makes it possible to identify both similarities and differences between them. More subtle differences will be identified and discussed later in the detailed analysis.

4. VARIATIONS OF DIFFERENT STRUCTURES IN THE SOUTHERN HEMISPHERE DURING HIGH SOLAR ACTIVITY

Figure 2 shows the longitude variations of different structures of the summer night ionosphere in the Southern Hemisphere. We used data from the CHAMP satellite for ICA obtained–on January 6-10, 2003. Figure 3 shows the latitudinal *fp* profile *s*obtained at different longitudes on January 7, 2003 for calm geomagnetic conditions (*Kp* varied from 1+ to 3 -). Data in the mid-to high-latitude region refer to the post-lunar ionosphere intηε ραvγε 0204 04 LT. The zones of auroral diffuse eruptions in Fig. 2 are shaded.

The asterisks in Figure 2 show the position of the *Ne* peak associated with WSA. The vertical lines show the width of this peak, but only for January 7, so as not to clutter the chart. The filled circles in Fig. 2 indicate the position of the GIP. The GIP is understood as a structure corresponding to the classical main ionospheric dip, i.e., a sufficiently deep minimum of electron concentration at typical latitudes of the GIP and the polar wall at the latitudes of precipitation in zone I. The polar wall of the GIP is indicated by triangles. A high-latitude dip is often observed more polar than the GIP; it is indicated by empty circles. VIP is usually observed inside the auroral oval, its polar wall is formed by diffuse eruptions in zone II. From Fig. 2 it can be seen that the classical HIP is clamped by the WSA in longitude on both sides, so that it is observed only in the longitude range 60-180° E. In fact, this is the main feature of the nighttime summer ionosphere of the Southern hemisphere. The thick curve also shows the position of the winter GIP for 04 LT [Karpachev et al., 2019]. It can be seen that the positions of the summer and winter dips do not differ much. At low longitudes, the GIP passes into a structure that is similar to a sinkhole, but its minimum is located much lower in latitude than the classical GIP and, accordingly, the equatorial edge of the auroral oval. Let's define this structure as a subgroup. Subprovals are indicated by squares in Fig. 2. They are observed in Fig. 3 on turns that correspond to longitudes 50, 26, and 3° E. E. The transition of the GIP to the SMS occurs so imperceptibly that it is easy to miss it during analysis. For example, the structure at longitude 60° E E in Figure 3 can be interpreted in two ways, both as a GIP and as a sub-gip. At this transition the polar wall of the GIP as at longitude 84° E E also imperceptibly passes into the plasma peak at longitude 50□° E, already explicitly linked to WSA. It follows from the above that the GIP/sms structure can be uniquely identified only in dynamics, considering the whole picture as shown in Figure 2.

WSA begins to develop at longitudes less than 60° E. A subplot is usually formed on the equatorial edge of the anomaly. With a further decrease in the longitude of observations, it becomes less noticeable and disappears during the transition to the Western Hemisphere. The WSA in the Western Hemisphere is the dominant structure; in Figure 2, it is bounded by a latitude –40oϕ 40 40°; in fact, it extends further to the equator, but in this case this is not essential. The

high-latitude edge of WSA in the Western Hemisphere is surprisingly close to the equatorial boundary of Zone I. However, this is quite natural, since the border of rashes almost coincides with plasmopause. The polar wind outside the plasmopause carries ionospheric plasma along the geomagnetic field lines up and further into the magnetosphere. Therefore, the polar boundary of the WSA is very sharp. Then the electron concentration decreases slowly and forms a minimum of VIP. Its polar wall is formed by eruptions in zone II. At low longitudes in the Eastern Hemisphere, the WSA is bounded not by the equatorial but by the polar boundary of zone I. This is because the WSA is just beginning to form at these longitudes, so that the effect of precipitation becomes noticeable at a low background level. In other words, in this case, the polar edge of the plasma peak is formed by diffuse eruptions.

VIP has a very variable structure, both in shape and position, so it is practically not reproduced when averaging data and is reflected on the map only in the longitude range of 120–180180 180° E. Similarly, the subplot is shown on the map together with the GIP only in the longitude rangeoϕ 3075° 75 E.

The dynamics of dips and WSA in the Southern summer hemisphere is so complex that it leads to contradictory results in its study. For example, in [Aa et al., 2020], statistical processing of data from the Swarm satellite showed that the summer dip in the Southern Hemisphere is on average located 1.4° more equatorially than the winter dip. In [Yang et al., 2018) As expected, the summer HIP was identified only in the longitude range of 60-90° but it turned out to be on average 3□ more equatorial than the winter dip. This is obviously due to the fact that in both cases, the data array also included a subproject that underestimated the average position of the GIP. In [Lee et al., 2011], data from the COSMIC/Formosat experiment were considered only outside the WSA zone, but the average position of the dip at 04 LT turned out to be much more polar than the winter GIP, at latitudes 64–6565 65–. It is not difficult to determine in Figure 2 that this corresponds to the VIP, and not the GIP.

Figure 3 shows the latitudinal *fp* profiles obtained at different longitudes on January 7, 2003. They were practically discussed in the process of describing fig. 2. Note again how smoothly the plasma peak forming the polar wall of the GIP is absorbed by the plasma peak during the formation of WSA. Note one more feature in Fig. 3. Let's note one more feature in Fig. 3. On the lowest fp profile obtained at longitude 212° E, the electron concentration slowly decreases towards high latitudes, forming a shallow VIP with a very low polar wall. Such latitudinal profiles are typical in the longitude rangeoϕ 150250° 250 E. E. VIP in this range of longitudes is maximally removed to the pole. This is probably due to the specific nature of eruptions in zone II in this longitude interval.

Figure 4.

For a more complete understanding of the morphology and causes of the formation of the nighttime summer ionosphere in the Southern Hemisphere, we will consider the most characteristic latitudinal sections *of fp* (Fig. 4. In Fig. 4a*a* shows a comparison of two sections - in the normal and anomalous ionosphere. Sections were obtained on January 9, 2003 in the longitude sectors 105° E and 335° E. At a longitudeoϕ 105 E E in the normal ionosphere, a classical hype is observed, the polar wall of which is formed by precipitation in zone I. HIP is also accompanied by a well-defined VIP, the polar wall of which is respectively formed by rashes in zone II. The positions of the rash zones correspond to the longitude of observations and *the Cr*-index. An extremely pronounced increase in the electron concentration associated with the formation of WSA is observed in the anomalous ionosphere. This increase reaches a maximum 9-10 MHz. The plasma peak abruptly ends at the latitude of the plasmopause, the VIP minimum is observed somewhat more polar, and its polar wall is located even further along the latitude. Thus, WSA completely absorbs the GIP, but does not affect the VIP, at least not much.

Figure*4b* shows the extremely characteristic latitudinal profile *fp* obtained on January 13, 2003 at longitude 22° E and the associated profile *fp* recorded in the Northern Hemisphere for almost the same conditions (dashed curve). In the Northern Hemisphere, a classic HYPO is observed with a minimum at latitude 62°. In the Southern Hemisphere, at the latitudes of the dip, at the same longitude 22° E E, a plasma peak associated with WSA begins to form. This peak is not strong enough to completely absorb the GIP, but it shifts the minimum of the GIP to the pole. This minimum is marked with a circle in Figure 4. A subplot is formed equatorially to WSA at latitude –50.5°, which is marked with a square. Note that no specific mechanism for the formation of subpoles was involved – the minimum electron concentration is formed simply because the concentration increases both to the equator and to the pole.

In Fig. 4b also shows the *fp* profiles in the Southern and conjugate Northern hemispheres. In the Northern Hemisphere, ISU is located at latitude 58°, which corresponds to longitude and *Cr*. In the Southern Hemisphere, at longitude 47° E, an anomaly begins to form, which fills the GIP minimum. Instead, a shallow minimum is formed, marked with a square. This minimum is located at latitude –52°, which is too low for the GIP, so it is a sub-level. In the conjugate Northern Hemisphere, a small peak of electron concentration is observed at these latitudes. The mechanism of formation of such a conjugate structure is well known – plasma flows from the summer hemisphere with an increased level of ionization along the magnetic force tube to the winter hemisphere due to diffusion (Krinberg and Tashchilin, 1984). This mechanism is most effective for mid-latitudes, where the volume of power tubes maximizes the flow of ionospheric plasma.

In Fig. 4*d* also shows the conjugate *fp* profiles obtained on January 8, 2003 in the longitude sector ~35° E. In the Northern Hemisphere, there is a well-defined HYPO. In the Southern Hemisphere, the WSA completely fills the GIP. And at very low latitudes - (43–47°), a minimum is observed, again conjugated with the plasma peak in the Northern winter Hemisphere.

Thus, we can distinguish two reasons for the formation of a subplot, which is quite regularly observed in the range of longitudes 0–60° E. One of them is related to the transfer of plasma from the summer hemisphere to the winter hemisphere under the influence of diffusion. The second reason is due to a sharp increase in the electron concentration to the pole during the formation of WSA, and in the presence of an increase in the concentration to the equator. In turn, the increase in the concentration towards the equator is associated either with the crest of the equatorial anomaly or with the local *Ne maximum* at low latitudes, which is usually observed even after the collapse of the equatorial anomaly [Karpachev, 2021].

5. VARIATIONS OF DIFFERENT STRUCTURES IN THE SOUTHERN HEMISPHERE DURING LOW SOLAR ACTIVITY

Consider the situation in the Southern Hemisphere with low solar activity and highlight its differences from high solar activity. Figure 5 shows the longitude variations of the Southern Hemisphere structures identified for January 3-11, 2008 for NSA and quiet geomagnetic conditions. The data refer to almost the same local time interval as in Figure 2 (03–04 LT). Figure 6 shows the latitudinal *fp* profiles typical of the NSA *fp*. Figure 6a*a*, similar to Fig. 4a, shows latitudinal profiles in the normal and anomalous ionosphere. In NSA, the increase in electron concentration at night in the WSA region reaches only 6 MHz compared to 10 MHz in ICA. GIP, on the contrary, is more pronounced in NSA. Therefore, the region of existence of classical GIP in HSA is wider than in ICA and occupies 0-225° E E, as can be seen in Figure 5. The weaker development of WSA also affects the fact that the polar boundary of all plasma peaks in Figure 5 is determined by diffuse precipitation, and not only at small longitudes, as shown in Fig. 5 with ICA (fig. 2). This is due to the fact that the effect of rashes becomes more noticeable at a low background level.

However, the main difference from ICA is the presence of sub-channels in the Western Hemisphere. Moreover, subprovals are observed at much lower latitudes than at ICA. Two examples of subwaves are shown in Figure 6*b*. The subwaves recorded on January 11, 2008 in the longitude sector 25° E at latitude –52°are similar to the subwaves observed at low longitudes in ICA. The subplot registered in the longitude sector 323° E is located at a very low latitude oϕ –37°. However, it stands out quite clearly, so it is impossible not to notice it when processing data. Especially if we are talking about automatic selection of dips. This technique has been increasingly used recently. Note that there are no sub-pipelines in the Western Hemisphere during ICA for a

simple reason – they are filled due to more intense solar ionization. But even with NSA, subprovals in the Western Hemisphere are not very pronounced.

The triangles in Fig. 5 mark the position of the polar wall of the GIP, which is formed as a separate peak. The polar wall of the HYPO, as usual, is associated with diffuse eruptions in zone I. In the longitude range−120-210 ° E,τηε πολαρ wall is still steep, but there are many plasma peaks at its top, which makes it difficult to determine its position, and it is not marked in Figure 5.

Figure 6.

Figure 6c is completely similar to Fig. 4b. In Fig. 6c shows the characteristic latitudinal profile of fp obtained on 5 January 2006 at the longitude 22° E and the conjugate profile of fp recorded in the Northern Hemisphere for almost the same conditions. In the Northern Hemisphere, a classical ISU with a minimum at latitude 62° is observed. In contrast, the Southern Hemisphere shows a plasma peak at these latitudes associated with WSA formation. Since the data refer to the midnight hours of local time, the WSA is not yet strongly developed and the plasma peak does not completely absorb the ISU. However, this peak shifts the minimum of the ISU to the pole and also forms a subwavelength at the latitude -50.5°.

Figure 6*(d*) shows the latitudinal *fp* profiles obtained on January 5, 2008 in the longitude sector 215° E. In the Southern Hemisphere, there is a well-defined subplot at latitude –47°. At approximately the same latitude, a plasma peak is observed in the Northern Hemisphere. Thus, the mechanism of plasma transfer from the summer hemisphere to the winter one works quite effectively even at low solar activity.

Horwath and Lowell (2009) studied the dip and WSA using data from the DMSP F15 satellite for the winter of 1996-1997, i.e. also for the NSA. The results obtained can be compared with ours. According to DMSP data, the plasmopause, GIP, WSA peak, and subpole were located at latitudes –62.5, –57.5, –56.2, and –42.5°, respectively. This is very close to what is observed in Fig. 5. The authors attributed the formation of a subplot to plasma stagnation and the influence of the South Atlantic magnetic anomaly. 6 of their article, the GIP and the subproject were represented as a single branch, i.e. they combined completely different structures into one whole. However, the high-latitude edge of the magnetic anomaly barely reaches −°35 GM GML at, so it is difficult to agree with its participation in the formation of subprovals. As for the stagnation of ionospheric plasma, it occurs at all latitudes and longitudes in the night ionosphere in the absence of solar ionization.

6. CONCLUSION

The contradictory results obtained on the ionization failure in the Southern summer hemisphere indicate a difficult situation to analyze. A detailed study of the structure of the summer night

(02–04 04 LT) ionosphere in the Southern Hemisphere fully confirmed this assumption. The complex behavior of the ionosphere under these conditions is determined by the Weddell Sea anomaly. Let's highlight the main provisions of the analysis.

– The plasma peak associated with the formation of WSA–reaches 6 MHz in 02-04 LT for HSA and 10 MHz for ICA.

– At WSA longitudes, this peak completely fills the main ionospheric dip. Therefore, GIP is observed only outside the WSA, at longitudes 60–180° E at ICA and 0–210° E at NSA.

– In ICA, the well-developed plasma peak associated with WSA drops sharply to the pole at the plasmopause latitude. This latitude almost coincides with the equatorial boundary of auroral diffuse eruptions. In HSA, the plasma peak associated with WSA is less strongly developed, so it expands to the pole due to diffuse eruptions in zone I. As a result, the combined peak is limited by the latitude of the polar boundary of diffuse eruptions in zone I. In other words, the polar boundary of the combined peak is determined by the degree of development of WSA. The boundaries of auroral diffuse eruptions were determined using the auroral oval model [Vorobjev et al., 2013].

– At the equatorial boundary of the WSA plasma peak, a subplot is often formed at latitudes much more equatorial than the classical GIP, up to ~35° GML at. In ICA, this subplot is observed only at the Eastern Hemisphere longitudes of 0–60° E, and in NSA, it is also observed in the Western Hemisphere. The subplot, especially in the Western Hemisphere, is poorly defined, located much more equatorially than the ISU, and, nevertheless, in some works it is confused with the ISU. Therefore, it cannot be excluded from the analysis.

– There are apparently two reasons for the formation of subpoenas. The first and simplest one is that the subpole minimum is formed with a sharp increase in the electron concentration to the pole during the formation of WSA, and to the equator – in the presence of an equatorial anomaly crest or its remnants. The second reason is related to the transfer of electron concentration from the summer hemisphere to the winter one. This mechanism is well known.

ACKNOWLEDGEMENTS

The author thanks the developers and operators of the CHAMP experiment (Deutsches GeoForschungs Zentrum (GFZ)) and the German Aerospace Center (DLR) for the data provided. CHAMP data is taken from the site https://isdc.gfz-potsdam.de/champ-isdc://isdc.gfz-potsdam.de/champ-isdc/.

REFERENCES

1. *Krinberg I.A., Tashchilin A.V.* Ionosphere and plasmosphere, Moscow: Nauka, 189 p. 1984.

2. *Karpachev A.T., Gasilov N.A., Karpachev O. A.* Morphology and causes of Weddell Sea anomaly // Geomagnetism and Aeronomy, vol. 51, No. 6, pp.−828-840, 2011.

3. Karpachev A.T. Diurnal and longitude variations of the equatorial anomaly for the winter solstice according to the Intercosmos-19 satellite // Geomagnetism and Aeronomy, vol. 61, no. 1, pp. 20-3−34. 2021. https://doi.org/10.31857/S://doi.org/10.31857/S0016794021010065

4. *Karpachev A.T.* Features of the structure of the winter morning ionosphere of high and middle latitudes // Geomagnetism and Aeronomy, VOL.63, NO. 6, PP.788-797, 2023. https://doi.org/10.31857/S0016794023600370.org/10.31857/S0016794023600370

5. *Aa E., Zou S., Erickson P. J., Zhang S.-R., Liu S.* Statistical analysis of the main ionospheric trough using Swarm in situ measurements // J. Geophys. Res. – Space. V. 125. N 3. ID e2019JA027583. 2020. https://doi.org/10.1029/2019JA027583

6. *Ahmed M., Sagalyn R.C., Wildman P.J.L., Burke W.J.* Topside ionospheric trough morphology: occurrence frequency and diurnal, seasonal and altitude variations // J. Geophys. Res. – Space. V. 84. N 2. P. 489–498. 1979. https://doi.org/10.1029/JA084iA02p00489

7. *Bellchambers W.H., Piggott W.R*. Ionospheric measurements made at Halley Bay // Nature. V. 182. N 4649. P. 1596–1597. 1958. https://doi.org/10.1038/1821596a0

8. *Burns A.G., Zeng Z., Wang W., Lei J., Solomon S.C., Richmond A.D., Killeen T.L., Kuo Y.-H.* The behavior of the *F*2 peak ionosphere over the South Pacific at dusk during quiet summer conditions from COSMIC data // J. Geophys. Res. – Space. V. 113. N 12. ID A12305. 2008. https://doi.org/10.1029/2008JA013308

9. *Dudeney J.R., Piggott W.R.* Antarctic ionospheric research / Upper Atmosphere Research in Antarctica / Antarctic Research Ser., 29. Eds. L.J. Lanzerotti, C.G. Park. Washington, DC: American Geophysical Union. P. 200–235. 1978. https://doi.org/10.1029/AR029p0200

10. *Grebowsky J.M., Tailor H.A., Lindsay J.M*. Location and source of ionospheric high latitude troughs // Planet. Space Sci. V. 31. N 1. P. 99–105. 1983. https://doi.org/10.1016/0032-0633(83)90034-X

11. *He M., Liu L., Wan W., Ning B., Zhao B., Wen J., Yue X., Le H.* A study of the Weddell Sea Anomaly observed by FORMOSAT-3/COSMIC // J. Geophys. Res. – Space. V. 114. N 12 ID A12309. 2009. https://doi.org/10.1029/2009JA014175

12. *Horvath I., Essex E.A.* The Weddell Sea Anomaly observed with the TOPEX satellite data // J. Atmos. Sol. Terr. Phys. V. 65. N. 6. P. 693–706. 2003. https://doi.org/10.1016/S1364-6826(03)00083-X.

13. *Horvath I.* A total electron content space weather study of the nighttime Weddell Sea Anomaly of 1996/1997 southern summer with TOPEX/Poseidon radar altimetry // J. Geophys. Res. – Space. V. 111. N 12. ID A12317. 2006. https://doi.org/10.1029/2006JA011679

14. *Horvath I., Lovell B.C.* Investigating the relationships among the South Atlantic Magnetic Anomaly, southern nighttime midlatitude trough, and nighttime Weddell Sea Anomaly during southern summer // J. Geophys. Res. – Space. V. 114. N 2. ID A02306. 2009. https://doi.org/10.1029/2008JA013719

15. *Jee G.. Burns A.G, Kim Y.-H., Wang W.* Seasonal and solar activity variations of the Weddell Sea Anomaly observed in the TOPEX total electron content measurements // J. Geophys. Res. – Space. V. 114. N 4. ID A04307. 2009. https://doi.org/10.1029/2008JA013801

16. *Karpachev A.T., Klimenko M.V., Klimenko V.V.* Longitudinal variations of the ionospheric trough position // Adv. Space Res. V. 63. N 2. P. 950–966. 2019. https://doi.org/10.1016/j.asr.2018.09.038

17. *Klimenko M.V., Klimenko V.V., Karpachev A.T., Ratovsky K.G., Stepanov A.E.* Spatial features of Weddell Sea and Yakutsk Anomalies in *foF*2 diurnal variations during high solar activity periods: Interkosmos-19 satellite and ground-based ionosonde observations, IRI reproduction and GSM TIP model simulation // Adv. Space Res. V. 55. N 8. P. 2020–2032. 2015. https://doi.org/10.1016/j.asr.2014.12.032

18. *Lee I.T., Wang W., Liu J.Y., Chen C.Y., Lin C.H.* The ionospheric midlatitude trough observed by FORMOSAT-3/COSMIC during solar minimum // J. Geophys. Res. – Space. V. 116. N 6. ID A06311. 2011. https://doi.org/10.1029/2010JA015544

19. *Liu H., Thampi S.V., Yamamoto M.* Phase reversal of the diurnal cycle in the midlatitude ionosphere // J. Geophys. Res. – Space. V. 115. N 1. ID A01305. 2010. https://doi.org/10.1029/2009JA014689

20. *Lin C.H., Liu J.Y., Cheng C.Z., Chen C.H., Liu C.H., Wang W., Burns A.G., Lei J.* Three-dimensional ionospheric electron density structure of the Weddell Sea Anomaly // J. Geophys. Res. – Space. V. 114. N 2. ID A02312. 2009. https://doi.org/10.1029/2008JA013455

21. *Moffett R.J., Quegan S.* The mid-latitude trough in the electron concentration of theionospheric *F*-layer: A review of observations and modeling // J. Atmos. Terr. Phys. V. 45. N 5. P. 315–343. 1983. https://doi.org/10.1016/S0021-9169(83)80038-5

22. *Muldrew D.B. F*-layer ionization troughs deduced from Alouette data // J. Geophys. Res. V. 70. N 11. P. 2635–2650. 1965. https://doi.org/10.1029/JZ070i011p02635

23. *Nilsson H., Sergienko T.I., Ebihara Y., Yamauchi M.* Quiet-time mid-latitude trough: influence of convection, field-aligned currents and proton precipitation // Ann. Geophys. V. 23. N 10. P. 3277–3288. 2005. https://doi.org/10.5194/angeo-23-3277-2005

24. *Penndorft R.* The average ionospheric conditions over the Antarctic / Geomagnetism and Aeronomy: Studies in the Ionosphere, Geomagnetism and Atmospheric Radio Noise / Antarctic Research Ser., 4. Ed. A.H.Waynick. Washington, DC: American Geophysical Union. P. 1–45. 1965. https://doi.org/10.1029/AR004p0001

25. *Richards P.G., Meier R.R., Chen S., Dandenault P.* Investigation of the causes of the longitudinal and solar cycle variation of the electron density in the Bering Sea and Weddell Sea anomalies // J. Geophys. Res. – Space. V. 123. N 9. P. 7825–7842. 2018. https://doi.org/10.1029/2018JA025413

26. *Rodger A.S., Moffett R.J, Quegan S.* The role of ion drift in the formation of ionisation troughs in the mid-and high-latitude ionosphere – a review // J. Atmos. Terr. Phys. V. 54. N 1. P. 1–30. 1992. https://doi.org/10.1016/0021-9169(92)90082-V

27. *Rother M., Michaelis I.* CH-ME-2-PLPT - CHAMP Electron density and temperature time series in low time resolution (Level 2). GFZ Data Services. 2019. https://doi.org/10.5880/GFZ.2.3.2019.007

28. *Vorobjev V.G., Yagodkina O.I., Katkalov Yu.V.* Auroral Precipitation Model and its applications to ionospheric and magnetospheric studies // J. Atmos. Sol.-Terr. Phy. V. 102. P. 157–171. 2013. http://dx.doi.org/10.1016/j.jastp.2013.05.007

29. *Williams P.J.S., Jain A.R.* Observations of the high latitude trough using EISCAT // J. Atmos. Terr. Phys. V. 48. N 5. P. 423–434. 1986. https://doi.org/10.1016/0021-9169(86)90119-4

30. *Yang N., Le H., Liu L., Zhang R.* Statistical behavior of the longitudinal variations of the evening topside mid-latitude trough position in both northern and southern hemispheres // J. Geophys. Res. – Space. V. 123. N 5. P. 3983–3997. 2018. https://doi.org/10.1029/2017JA025048

FIGURE CAPTIONS

Figure 1. Distribution *of the fp plasma frequency* according to the CHAMP satellite data in the Southern Summer hemisphere in January 2003 and January 2008. Local time 02–04 h. The dashed curve shows the position of the GIP minimum for 04 LT in winter conditions.

2. Longitude variations according to CHAMP data for high solar activity in January 2003 of the positions of the VIP (empty circles), GIP (filled circles), the polar wall of the GIP (triangles), the subplot (squares), and the WSA peak (asterisks). Zones I and II of auroral diffuse eruptions are shaded according to the model [Vorobjev et al., 2013]. The vertical lines represent WSA for January 7. Local time 02–04 hours The thick curve shows the position of the GIP for 04 LT, but in winter conditions.

Figure 3. Latitudinal sections *of fp* in different longitude sectors obtained from CHAMP data on January 7, 2003. Filled circles indicate the position of the GIP, empty circles indicate the position of the VIP, and squares indicate the position of the subplot. For convenience, the corresponding longitude sectors are indicated for the three Y-axes on the left.

4. Typical latitudinal sections *of fp* for different conditions in the Southern and Northern hemispheres. For each case, the date, local time, longitude, and *Kp*-ZIP code are specified. Dashed curves refer to the Northern Hemisphere. The position of the GIP is marked with a filled circle, the VIP - with an empty circle, and the subpart-with a square.

5. Longitude variations according to CHAMP data for low solar activity in January 2008 of the position of the VIP (empty circles), GIP (filled circles), the polar wall of the GIP (triangles), the subplot (squares), and the WSA peak (asterisks). The vertical lines represent the WSA for January 10. Zones I and II of auroral diffuse eruptions are shaded according to the model [Vorobjev et al., 2013]. Local time 03–04 hours The thick curve shows the position of the GIP for 04 LT, but in winter conditions.

6. Typical latitudinal sections *of fp* for different conditions in the Southern and Northern hemispheres. For each case, the date, local time, longitude, and *Kp*ZIP code are specified. Dashed curves refer to the Northern Hemisphere. The position of the GIP is marked with a filled circle, the VIP - with an empty circle, and the subpart-with a square.

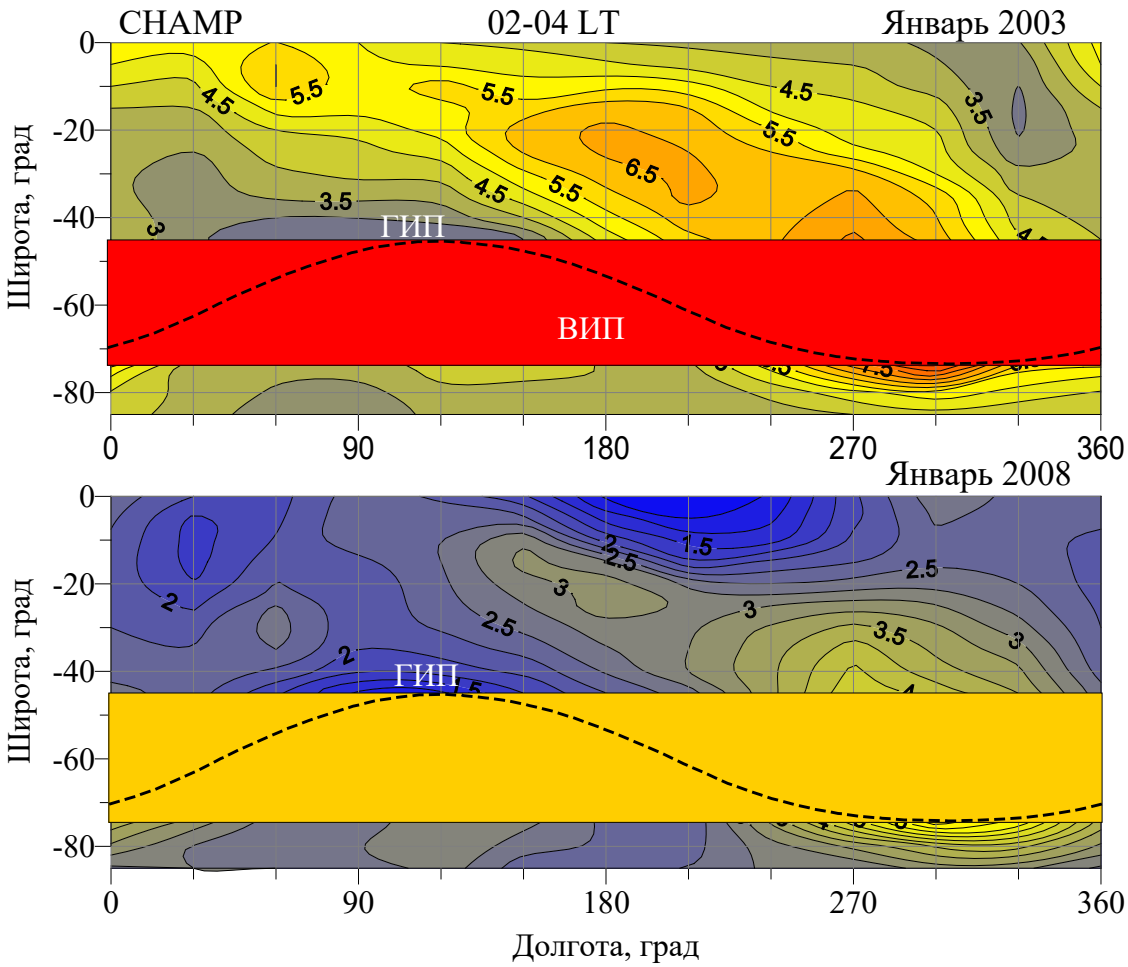
CHAMP
02-04 LT
Январь 2003
Широта, град
ГИП
ВИП
Январь 2008
Широта, град
ГИП
Долгота, град

Figure 1.

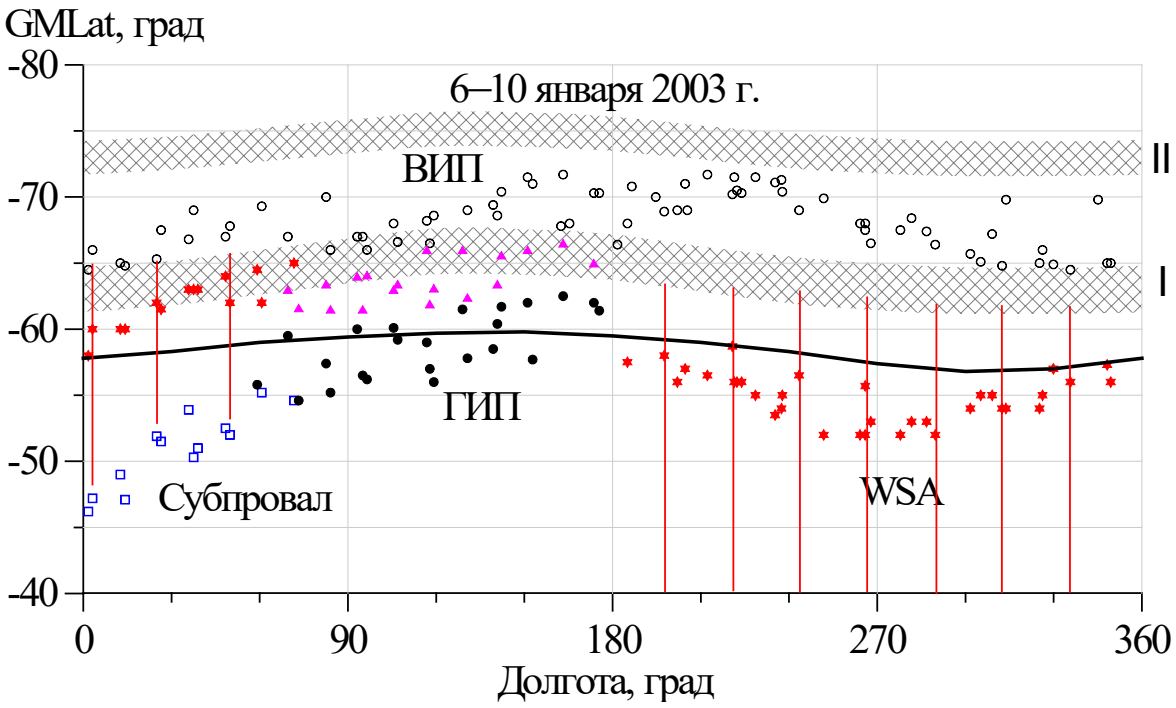
GMLat, град
-80
-70
-60
-50
-40
6–10 января 2003 г.
ВИП
II
I
ГИП
Субпровал
WSA
0
90
180
270
360
Долгота, град

Figure 2.

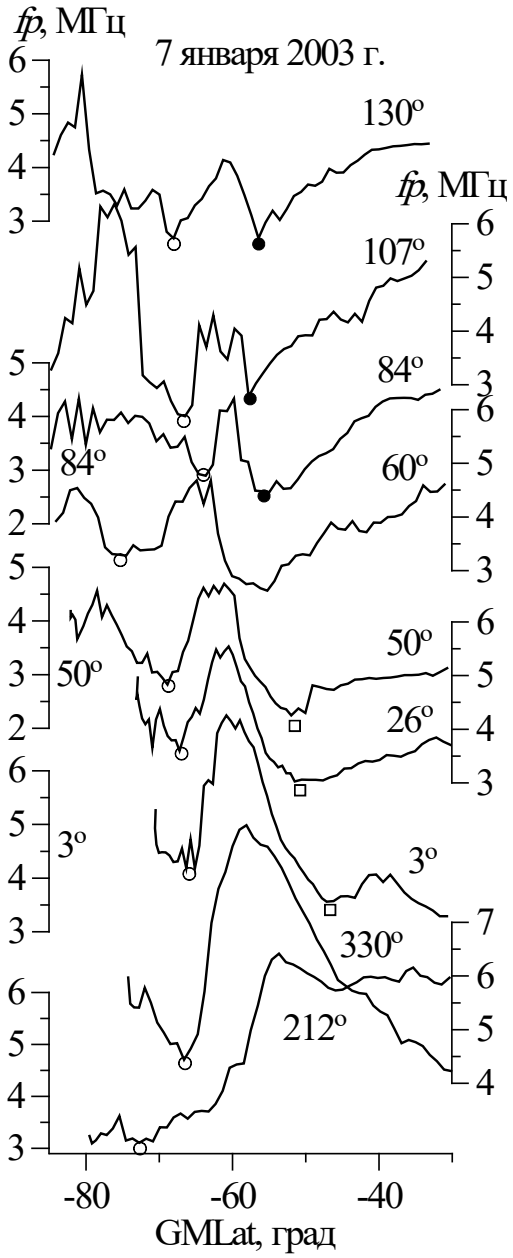
fp, МГц
7 января 2003 г.
130°
fp, МГц
107°
84°
84°
60°
50°
50°
26°
3°
3°
330°
212°
-80
-60
-40
GMLat, град

Figure 3.

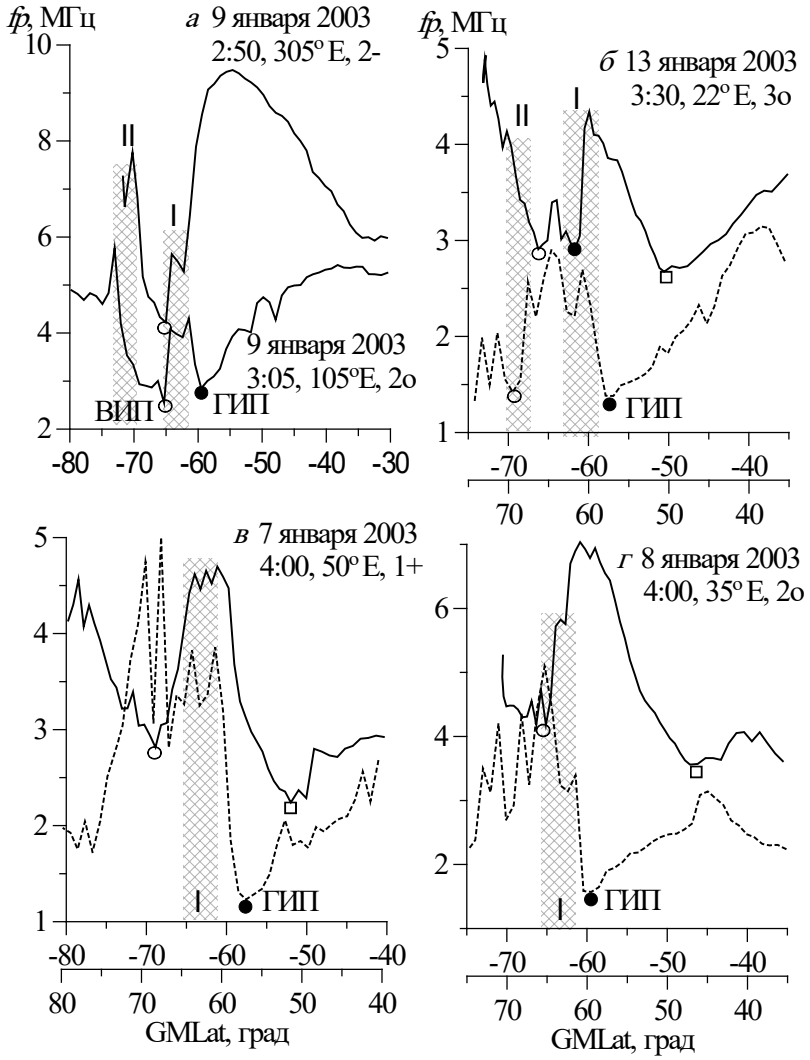
fp, МГц
а 9 января 2003
2:50, 305° E, 2-
II
I
9 января 2003
3:05, 105°E, 2o
ВИП
ГИП
б 13 января 2003
3:30, 22° E, 3o
в 7 января 2003
4:00, 50° E, 1+
г 8 января 2003
4:00, 35° E, 2o
GMLat, град

Figure 4.

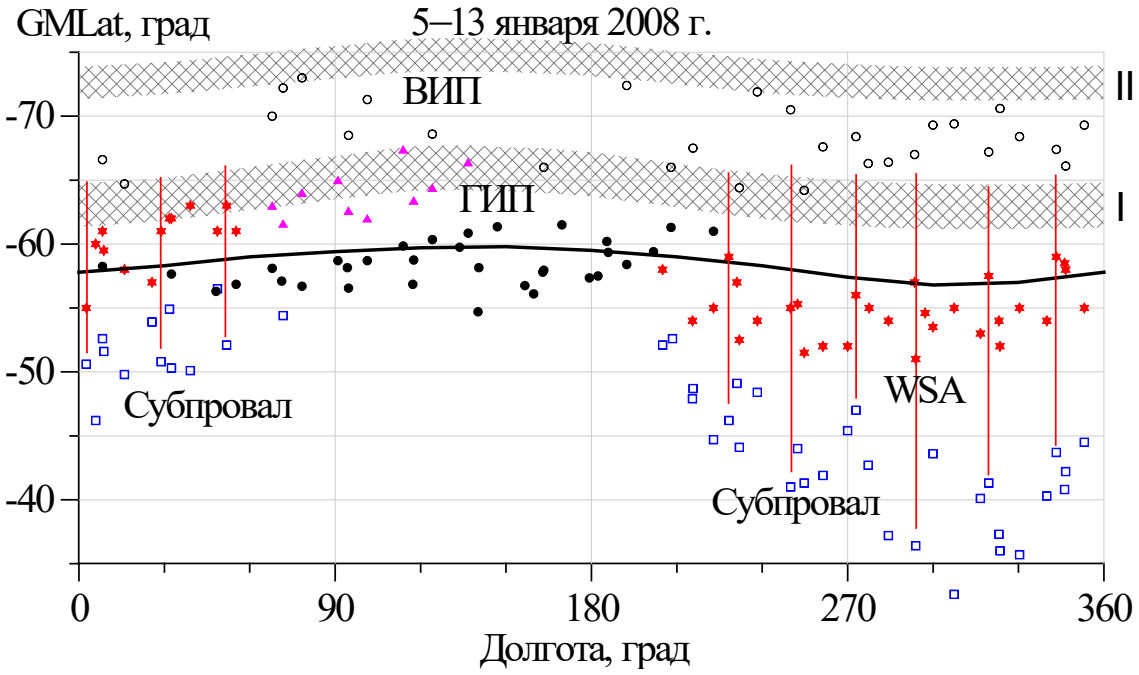
GMLat, град
5–13 января 2008 г.
ВИП
ГИП
II
I
-70
-60
-50
-40
Субпровал
WSA
Субпровал
0
90
180
270
360
Долгота, град

Figure 5.

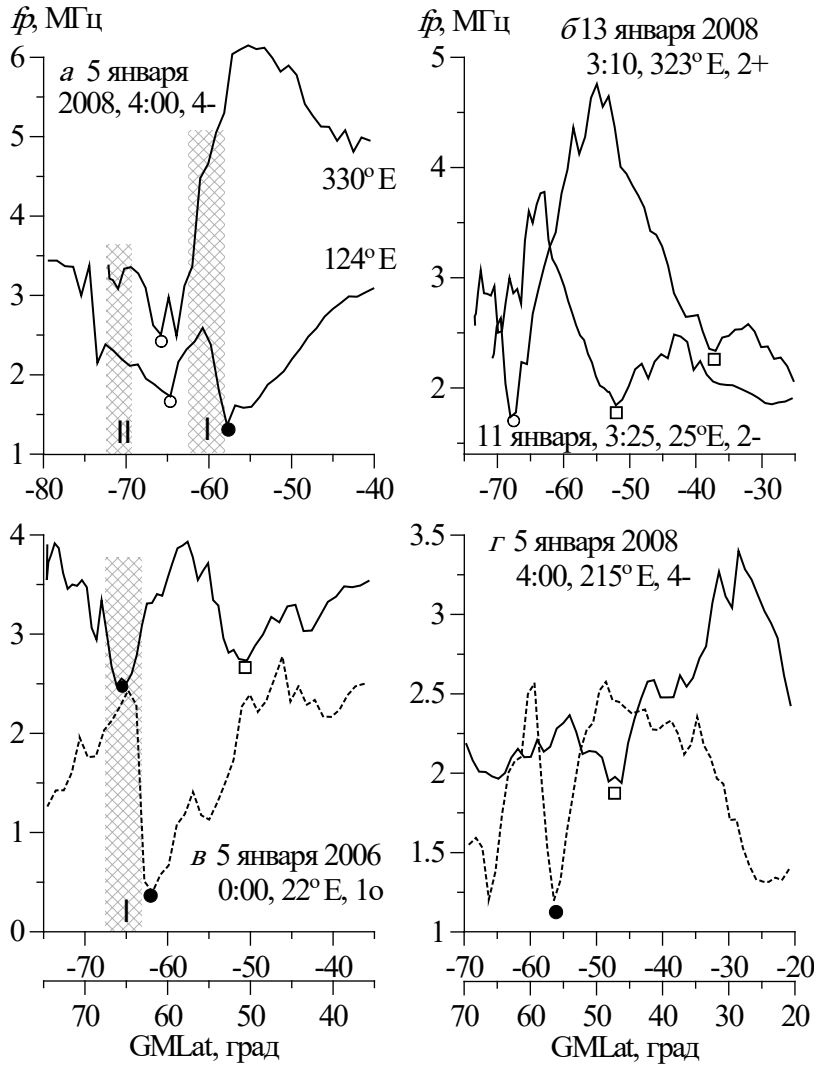
fp, МГц
а 5 января
2008, 4:00, 4-
330° E
124° E
II
I
fp, МГц
б 13 января 2008
3:10, 323° E, 2+
11 января, 3:25, 25°E, 2-
в 5 января 2006
0:00, 22° E, 1o
I
г 5 января 2008
4:00, 215° E, 4-
GMLat, град
GMLat, град

Figure 6.